Estimation of Equivalent Current Distribution Using Fourier Transform and Eigenmode Currents

Kazuto Mochiki, Keisuke Konno, *Member, IEEE*, and Qiang Chen, *Senior Member, IEEE*

***Abstract*—The estimation of the equivalent current distribution is a challenge when the precise geometry of the real source is unknown. In this study, a novel estimation method for the equivalent current distribution is proposed. The proposed method is a hybrid of the Fourier transform and eigenmode currents of equivalent sources. The equivalent current distribution is estimated using the proposed method as follows. First, the Fourier transform is applied to an electric field integral equation, and the initial equivalent current distribution on a specific estimation plane is estimated from the near-field data of the real source. Utilizing the initial equivalent current distribution, the equivalent sources that are uniformly arranged over the estimation plane are thinned. Subsequently, the equivalent current distribution is estimated using a matrix equation and the eigenmode currents of the remaining equivalent sources. The advantages of the proposed method are as follows. First, the precise geometry of the real source is not needed during estimation. Second, the number of equivalent sources is reduced, and the estimation of the equivalent current distribution is well conditioned. The performance of the proposed method is validated both numerically and experimentally. Empirical guidelines for threshold values for thinning equivalent sources are provided.**

***Index Terms*—Eigenmode currents, equivalent source, Fourier transform, inverse problem, method of moments (MoM).**

I. Introduction

RECENTLY, unintentional radiation from electronic devices has become a serious problem [1], [2]. Unintentionally radiated electromagnetic waves can interfere with surrounding electronic devices and, thus, must be suppressed. A source reconstruction method is commonly applied in determining the source of electromagnetic waves radiating from electronic devices. Once the source is identified, the unintentionally radiated electromagnetic waves from the source can be suppressed.

Source reconstruction is an inverse problem, and extensive effort has been dedicated to developing source reconstruction methods. Moreover, source reconstruction methods using equivalent sources have been proposed. Using integral equation approaches, the equivalent sources are reconstructed from the measured field data. Source reconstruction on 3-D surfaces has been demonstrated using different integral equation formulations, and its accuracy has been validated [3]–[5]. Near-field to far-field transformation techniques using equivalent magnetic currents have been proposed [6], [7]. The far-field of array antennas can be calculated from reconstructed magnetic currents. Near-field to far-field transformation techniques using equivalent sources have been enhanced, making them applicable to phaseless near-field data [8], [9]. A method for estimating the current distribution on a microstrip line of a multilayer printed circuit board from measured near-field data has been proposed [10], [11]. Guidelines for setting parameters for near-field measurement and dealing with lumped elements on the microstrip line have also been clarified. A method for estimating the equivalent sources of modulated EM radiation sources was proposed, and the equivalent sources of a microwave oven were estimated [12]. The time-domain near-field method is used for measuring the modulated EM wave in the time domain [13], [14], and its equivalent sources are estimated from the measured near-field data in the frequency domain. In recent years, a source reconstruction method based on Poggio–Miller–Chang–Harrington–Wu formulation with a probe correction technique has been proposed for noninvasive specific absorption rate measurements inside a dielectric object [15].

Source reconstruction necessitates overcoming ill posedness [16]. Regularization techniques have been introduced to alleviate the ill posedness of source reconstruction, [17]–[19]. The norm of the source vector to be reconstructed is added to the cost functions, and the resultant source reconstruction problem is well conditioned. In recent years, eigenmode current-based approaches have been proposed to alleviate the ill posedness of the source reconstruction of array antennas [20], [21]. Because the eigenmode currents of the array antennas can be used as macro basis functions, the current to be reconstructed is expanded using eigenmode currents. It has been demonstrated that the source reconstruction problem is well conditioned when a moderate number of eigenmode currents are used. Moreover, eigenmode currents have been applied to nonlinear inverse problems using an artificial neural network (ANN) [22]. Notably, these eigenmode current-based approaches are only applicable to the reconstruction of real sources with known geometries.

Although such advancements in source reconstruction methods have been demonstrated, unknown or imprecise geometries pose a challenge. When the precise geometry of the real source is unknown, the equivalent sources are arranged over the entire area where the real source is suspected. Therefore, the number

Manuscript received July 31, 2021; revised November 1, 2021 and March 10, 2022; accepted April 29, 2022. This work was supported by JSPS KAKENHI under Grants 18K13736 and 22K04061. (*Corresponding author: Keisuke Konno.*)

The authors are with the Department of Electrical and Communications Engineering, Graduate School of Engineering, Tohoku University, Miyagi 980-8577, Japan (e-mail: kazuto.mochiki.t5@alumni.tohoku.ac.jp; keisuke.konno.b5@tohoku.ac.jp; chenq@ecei.tohoku.ac.jp).

Color versions of one or more figures in this article are available at https://doi.org/10.1109/TEMC.2022.3172137.

Digital Object Identifier 10.1109/TEMC.2022.3172137

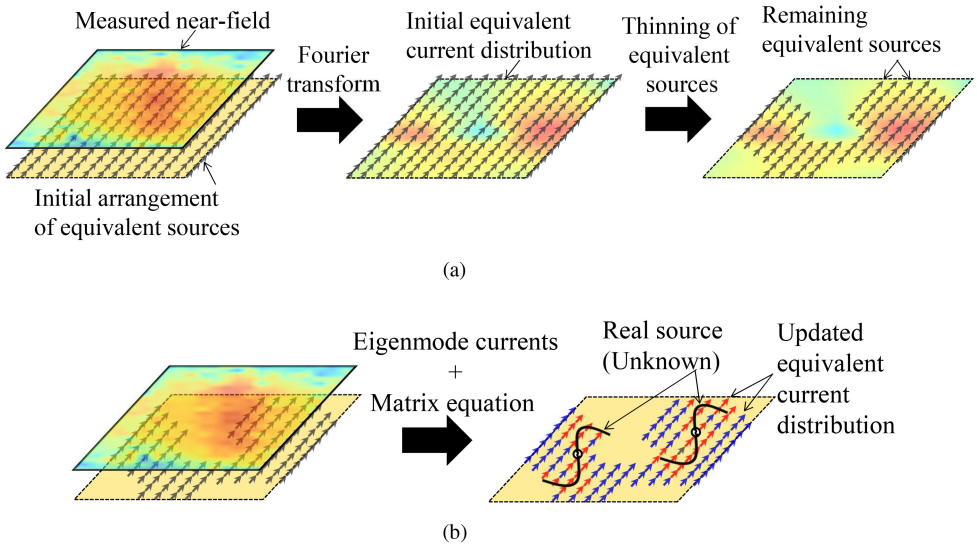

Fig. 1. Algorithm of proposed method. (a) Current obtained using Fourier transform and thinning of equivalent sources. (b) Estimation of the equivalent current distribution of the remaining equivalent sources.

of equivalent sources during the source reconstruction becomes large, and the source reconstruction suffers from ill posedness.

In this article, a novel estimation method for the equivalent current distribution for a source whose precise geometry is unknown is proposed. It is a hybrid method that combines the Fourier transform [8] and the eigenmode currents of the equivalent sources. Further, the equivalent sources are thinned prior to determining their equivalent current distributions. Thus, the source reconstruction problem is well conditioned, although the precise geometry of the real source is unknown. It should be noted that operating frequency of the source is expected to be known prior to applying the proposed method. Therefore, the proposed method is applicable to finding the continuous wave (CW) source. For example, the proposed method can be applied to identifying multiple CW sources inside wireless devices (e.g., radiation from an antenna and leakage from microwave components).

The rest of this article is organized as follows. In Section II, the algorithm of the proposed method is described in detail. Its performance is demonstrated numerically in Section III. In Section IV, the equivalent current distribution of the fabricated antenna prototype is estimated using the proposed method. Finally, Section V concludes this article.

II. Proposed Method

The algorithm for the proposed method is illustrated in Fig. 1. The proposed method is based on EFIE because our in-house code for the method of moments (MoM) is based on EFIE [23]. In the proposed method, the equivalent current distribution of the equivalent sources is obtained as follows. First, the near-field data of the real source are measured over a specific measurement plane. A Fourier transform is applied to the EFIE, and the initial equivalent current distribution on a specific estimation plane is estimated from the measured near-field data. Next, equivalent sources (i.e., small dipole elements) are uniformly arranged over the estimation plane (i.e., the equivalent sources are arranged over the same plane as the initial equivalent current), and their eigenmode currents are obtained. The contribution of the equivalent sources to the initial equivalent current distribution is evaluated, according to the initial equivalent current distribution and the eigenmode currents. Subsequently, the equivalent sources whose contribution to the initial current distribution is small are thinned. Subsequently, the equivalent current distribution of the remaining equivalent sources is decomposed into their eigenmode currents. Their unknown weight coefficients are obtained from a matrix equation and the equivalent current distribution is estimated. Notably, the method proposed here focuses on estimation of the equivalent current distribution of the planar real source. Theoretically, the equivalent current distribution of a complicated three-dimensional real source can be estimated in a manner similar to that of the proposed method. For a complicated 3-D real source, the equivalent sources should be arranged inside a specific volume.

A. Estimation of Initial Equivalent Current Distribution Using Fourier Transform

The near-field $\boldsymbol{E}(\boldsymbol{r})$ of the real source is measured using a probe scanning on the measurement plane. The current over the estimation plane S' is $\boldsymbol{J}(\boldsymbol{r}')$, and the current is assumed to be a source of the measured near-field $\boldsymbol{E}(\boldsymbol{r})$. The relationship between the current $\boldsymbol{J}(\boldsymbol{r}')$ and the measured near-field $\boldsymbol{E}(\boldsymbol{r})$ is described using the EFIE as follows:

$$\boldsymbol{E}(\boldsymbol{r}) = -j\omega\mu_0 \iint_{S'} \overline{\boldsymbol{G}}(\boldsymbol{r}, \boldsymbol{r}') \cdot \boldsymbol{J}(\boldsymbol{r}') dS' \tag{1}$$

where $\boldsymbol{r} = (x, y, z)$ and $\boldsymbol{r}' = (x', y', z')$ are the position vectors of the observation point and source, respectively. $\overline{\boldsymbol{G}}(\boldsymbol{r}, \boldsymbol{r}')$ is the

dyadic Green's function of free space

$$\overline{\boldsymbol{G}}(\boldsymbol{r},\boldsymbol{r}') = \left(\overline{\boldsymbol{I}} + \frac{\nabla\nabla}{k_0^2}\right)\frac{e^{-jk_0|\boldsymbol{r}-\boldsymbol{r}'|}}{4\pi|\boldsymbol{r}-\boldsymbol{r}'|} \tag{2}$$

where k_0 is a wavenumber of the free-space.

Because (1) is a so-called convolution integral, the following expression is obtained after a Fourier transform is applied to both sides of (1):

$$\tilde{\boldsymbol{E}}(\boldsymbol{k}) = \tilde{\overline{\boldsymbol{G}}}(\boldsymbol{k}) \cdot \tilde{\boldsymbol{J}}(\boldsymbol{k}) \tag{3}$$

where $\tilde{}$ indicates a physical quantity that is transformed from the spatial domain to the spectral domain using Fourier transform. $\boldsymbol{k}$ denotes the wavenumber vector in the spectral domain. Generally, (3) is a 3×3 matrix equation and can be solved easily as follows:

$$\boldsymbol{J}(\boldsymbol{r}') = \mathcal{F}^{-1}[\tilde{\overline{\boldsymbol{G}}}(\boldsymbol{k})^{-1} \cdot \tilde{\boldsymbol{E}}(\boldsymbol{k})]. \tag{4}$$

The current $\boldsymbol{J}(\boldsymbol{r}')$ obtained here is the initial equivalent current distribution on the estimation plane. The details of the Fourier transform used in this study are available in the Appendix. Notably, $\boldsymbol{J}(\boldsymbol{r}')$ in (4) can be uniquely obtained for ideal inverse problems. However, $\boldsymbol{J}(\boldsymbol{r}')$ is not uniquely obtained for practical inverse problems owing to the measurement error, noise, and the difficulty in near-field sampling over a closed surface. Therefore, $\boldsymbol{J}(\boldsymbol{r}')$ is the initial equivalent current distribution, which is updated using eigenmode currents.

The initial equivalent current distribution obtained here directly affects the value of the threshold η which is mentioned in the Section II-B. Because the threshold η affects the arrangement of the updated equivalent sources, the initial equivalent current distribution should be obtained such that it reflects the current distribution of the real source. In practice, some remedies may be helpful in reflecting the current distribution of the real source to the initial equivalent current distribution. For example, averaging the measured electric field, measuring over the plane enclosing the real source, and using Greens function including surrounding scatterers (i.e., ground plane or layered media) are expected to be helpful.

B. Thinning of Equivalent Sources

Here, the arrangement of equivalent sources over the estimation plane is obtained such that it reflects the initial equivalent current distribution $\boldsymbol{J}(\boldsymbol{r}')$. First, the equivalent sources, that is, the small dipole elements, are arranged uniformly over the estimation plane. Subsequently, N_i-dimensional current vector $\boldsymbol{J}_{N_i}$ corresponding to the equivalent sources is obtained using (4)

$$\mathbf{J}_{N_i} = [J_1, \ldots, J_{n_i}, \ldots, J_{N_i}]^T \tag{5}$$

where N_i denotes the initial number of equivalent sources. Next, an impedance matrix $\boldsymbol{Z}_{N_i \times N_i}$ of the equivalent sources is obtained using the method of moments (MoM) [23], [24]. Once the impedance matrix is obtained using Galerkin's method, the reciprocal of the impedance matrix is obtained, and $\boldsymbol{Z}^{\dagger}_{N_i \times N_i}\boldsymbol{Z}_{N_i \times N_i}$ becomes a Hermitian matrix. It is well known that eigenvectors of a Hermitian matrix are orthonormal to each other. Therefore, eigenvectors $\boldsymbol{e}_{n_i}(1 \le n_i \le N_i)$ of $\boldsymbol{Z}^{\dagger}_{N_i \times N_i}\boldsymbol{Z}_{N_i \times N_i}$ can be used as the entire domain basis functions for equivalent sources. The eigenvectors are called eigenmode currents [25]–[28]. Notably, orthonormal sets of vectors can be used as entire domain basis functions, and the choice of sets of orthonormal vectors is not limited to those of this approach.

To update the arrangement of equivalent sources, the contribution of each equivalent source to the initial equivalent current distribution is calculated as follows:

$$\eta_{n_i} = \sum_{k=1}^{N_i} |J_{n_i} e_{n_i,k}| \tag{6}$$

where J_{n_i} is the current of the n_ith equivalent source obtained using the Fourier transform and $e_{n_i,k}$ is the n_ith component of the kth eigenmode current. It can be found that η_{n_i} is the total contribution of the n_ith equivalent source to the initial equivalent current distribution. Moreover, η_{n_i} indicates the contribution of the n_ith equivalent source to the eigenmode current. Therefore, the equivalent source (i.e., dipole element) whose contribution to both the initial current distribution and dominant eigenmode current is large can be found according to η_{n_i}. Finally, η_{n_i} is normalized by its maximum $\eta_{\max}$ and equivalent sources whose contribution to the initial equivalent current distribution is smaller than the threshold η are thinned

$$\frac{\eta_{n_i}}{\eta_{\max}} < \eta. \tag{7}$$

As shown in Fig. 1(a), updated arrangement of the equivalent sources obtained in this manner should reflect the initial equivalent current distribution. Because the initial equivalent current distribution is obtained from the near-field of the real source, the remaining equivalent sources are relevant to the current of the real source, whereas the initial equivalent sources are not. Consequently, the eigenmode currents of the remaining equivalent sources are expected to be helpful to expanding the current of the real source. Moreover, the number of equivalent sources can be reduced, and the estimation of the equivalent current distribution is well conditioned.

C. Estimation of Equivalent Current Distribution Using Eigenmode Currents and Matrix Equation

Here, the estimation of the equivalent current distribution is performed using the eigenmode currents of the remaining equivalent sources. The eigenmode currents of the remaining equivalent sources are obtained from their impedance matrix $\boldsymbol{Z}_{N \times N}$ using the MoM, where N is the number of remaining equivalent sources. The current $\boldsymbol{I}_N$ of the remaining equivalent sources is expanded using their eigenmode currents $\boldsymbol{e}_n(1 \le n \le N)$, as follows:

$$\boldsymbol{I}_N \approx \sum_{l=1}^{L} \alpha_l \boldsymbol{e}_l \tag{8}$$

where $\boldsymbol{e}_l$ is the lth eigenmode current of the remaining equivalent sources, α_l is the unknown weight coefficient, and $L(L \le N)$ is the number of eigenmode currents used to expand the current

distribution. It was previously demonstrated that the contribution of the eigenmode current to the current is large when its eigenvalue is small [25]. Therefore, in this study, L-eigenmode currents with relatively small eigenvalues were used to expand the current distribution.

The unknown weight coefficients α_l can be obtained numerically by solving the following matrix equation. A probe was scanned over the measurement plane, and the near-field was measured at P measurement points. The receiving voltages of the probe at the P measurement points were stored in $\boldsymbol{V}_P$ as a complex voltage vector. The mutual impedances between the probe and equivalent sources can be obtained using the MoM, and the resultant $P \times N$ mutual impedance matrix $\boldsymbol{Z}_{P\times N}$ is expressed as follows:

$$\boldsymbol{Z}_{P\times N} = \begin{bmatrix} Z_{11} & \cdots & Z_{1N} \\ \ddots & & \\ \vdots & Z_{pn} & \vdots \\ & \ddots & \\ Z_{P1} & \cdots & Z_{PN} \end{bmatrix} \tag{9}$$

where Z_{pn} is the mutual impedance between the probe at the pth measurement point and the nth equivalent source. Thus, the following matrix equation is obtained:

$$\boldsymbol{Z}_{P\times N}\boldsymbol{I}_N = \boldsymbol{V}_P. \tag{10}$$

Once (8) is substituted into (10), the following matrix equation is readily obtained:

$$\boldsymbol{Z}_{P\times N}\sum_{l=1}^{L}\alpha_l\boldsymbol{e}_l = \boldsymbol{V}_P$$

$$\sum_{l=1}^{L}\alpha_l\left(\boldsymbol{Z}_{P\times N}\boldsymbol{e}_l\right) = \boldsymbol{V}_P$$

$$\boldsymbol{Z}'_{P\times L}\boldsymbol{a}_L = \boldsymbol{V}_P. \tag{11}$$

Here

$$\boldsymbol{Z}'_{P\times L} = \begin{bmatrix} \sum_{n=1}^{N} Z_{1n}e_{1n} & \sum_{n=1}^{N} Z_{1n}e_{2n} & \cdots & \sum_{n=1}^{N} Z_{1n}e_{Ln} \\ \vdots & \vdots & \ddots & \vdots \\ \sum_{n=1}^{N} Z_{Pn}e_{1n} & \sum_{n=1}^{N} Z_{Pn}e_{2n} & \cdots & \sum_{n=1}^{N} Z_{Pn}e_{Ln} \end{bmatrix} \tag{12}$$

$$\boldsymbol{a}_L = \begin{bmatrix} \alpha_1 \\ \alpha_2 \\ \vdots \\ \alpha_L \end{bmatrix} \tag{13}$$

where $\boldsymbol{a}_L$ is a vector of the unknown weight coefficients. $\boldsymbol{Z}'_{P\times L}$ is a $P \times L$ matrix and not a square matrix when $P \neq L$. Therefore, (11) is solved using a singular value decomposition and unknown weight coefficients α_l are obtained. Finally, the eigenmode currents $\boldsymbol{e}_l$ and their weight coefficients α_l are substituted into (8), the equivalent current distribution of the remaining equivalent sources is obtained as shown in Fig. 1(b).

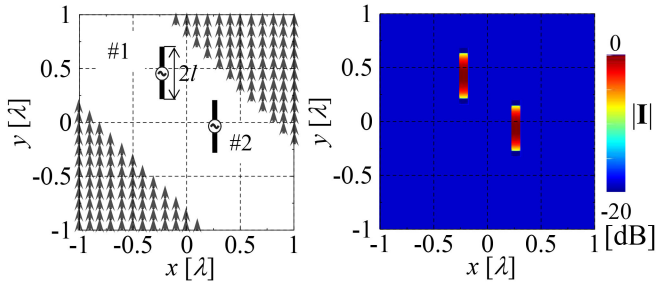

Fig. 2. Dipole array antenna (two elements) and its current distribution.

Notably, both $\boldsymbol{J}(\boldsymbol{r}')$ and $\boldsymbol{I}_N$ are EFIE solutions. However, both are equivalent current distributions (i.e., the near-field from both are equivalent to that from the real source) and not always coincident with the real sources themselves.

III. Numerical Simulation

Here, the performance of the proposed method is demonstrated via numerical simulation. As shown in Fig. 1, the near-field on a specific measurement plane is scanned, and the equivalent current distribution of the equivalent sources is estimated. To simplify the measurement of the near-field, only the y-component of the near-field ($= E_y$) is measured, and the y-component of the equivalent current distribution ($=J_y$ and I_y) is estimated throughout this study. As expected, multiple components of the near-field can be used to estimate the equivalent current distribution at the expense of the estimation cost, such as the measurement time or computational resources. The equivalent sources are small dipole arrays that are parallel to the y-axis, and (4) is reduced from a matrix equation to a scalar equation, that is, $J_y = \mathcal{F}^{-1}[\frac{\tilde{E}_y}{\tilde{g}_{yy}}]$, where $\tilde{g}_{yy}$ is a Fourier transformed yy-component of the dyadic Green's function in free space. As mentioned in Section I, the proposed method is applicable to finding multiple CW sources. Here, multiple antenna elements, which are the simplest models of multiple CW sources, are used as numerical examples. The equivalent current distribution is estimated for two real source models: a dipole array antenna and a loop array antenna. The two real source models and their current distributions obtained using the MoM are shown in Figs. 2 and 3, respectively. The dipole antenna and loop antenna are discretized into 5 and 24 linear current segments, respectively, during numerical analysis using the MoM. The geometry of the real/equivalent sources and the definition of the parameters for the numerical simulation are shown in Figs. 4, 5, and Table I. Although many parameters are provided for the proposed method, only two parameters, η and L, are optimized here. The remaining parameters are given to satisfy the Nyquist sampling theorem. The frequency of the real source was assumed to be known. Moreover, as prior knowledge, the approximate size of the area where the real source is expected

TABLE I
GEOMETRY OF REAL/EQUIVALENT SOURCES AND PARAMETERS FOR NUMERICAL SIMULATION

Real source	Dipole array antenna	Loop array antenna
Number of elements	2	3
Length of elements	$2l = 0.5\lambda$	$l_x = l_y = 0.3\lambda$
Feeding points (x, y)	#1 $(-0.2\lambda, 0.45\lambda)$, #2 $(0.3\lambda, -0.05\lambda)$	#1 $(0, -0.5\lambda)$, #2 $(0, 0)$, #3 $(0, 0.5\lambda)$
Feeding	Uniform and in-phase	
Length of probe	$l_p = 0.1\lambda$	
Spacing between measurement and estimation planes	$h = 0.1\lambda$	
Interval of measurement points	$\Delta p_x = \Delta p_y = 0.1\lambda$	$\Delta p_x = \Delta p_y = 0.08\lambda$
Number of measurement points	$P = 21 \times 21 = 441$	$P = 25 \times 25 = 625$
Signal to noise ratio	SNR $= 20$ dB	
Length of equivalent source	$l_h = 0.1\lambda$	
Radius of source and equivalent source	$a = 0.001\lambda$	$a = 0.01\lambda$
Spacing between equivalent sources	$\Delta x' = \Delta y' = 0.1\lambda$	
Area of estimation and measurement planes	$w_x \times w_y = 2\lambda \times 2\lambda$	
Threshold	η dB	
Initial number of equivalent sources	$N_i = 441 (= 21 \times 21)$	
Number of equivalent sources	$N = 16@\eta = -5$, $N = 146@\eta = -15$ $N = 359@\eta = -20$, $N = N_i@\eta = -\infty$	$N = 25@\eta = -15$, $N = 96@\eta = -25$ $N = 211@\eta = -30$, $N = N_i@\eta = -\infty$

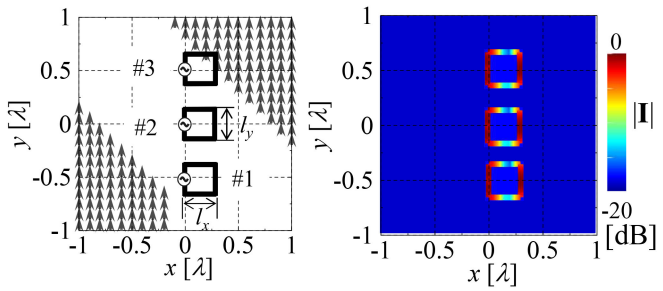

Fig. 3. Loop array antenna (three elements) and its current distribution.

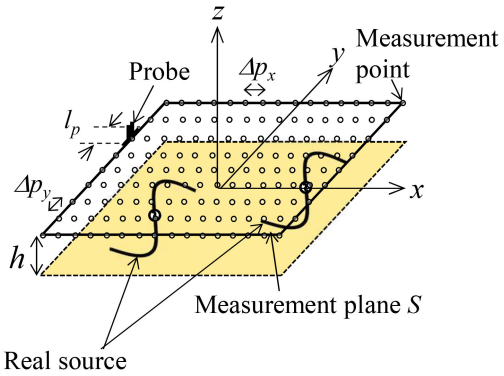

Fig. 4. Near-field measurement model.

to be, may be helpful for setting the remaining parameters, such as the area of the estimation/measurement planes.

The accuracy of the estimation was evaluated using the following two criteria. The first is a condition number κ defined as follows:

$$\kappa = \frac{\sigma_{\max}}{\sigma_{\min}} \tag{14}$$

where $\sigma_{\max}$ and $\sigma_{\min}$ are the maximum and minimum singular values of the matrix $\boldsymbol{Z}'_{P\times L}$ in (11), respectively. A small κ value indicates that the estimation of the equivalent current distribution is a well-conditioned problem. The latter is numerically stable because its solution is robust to the effect of

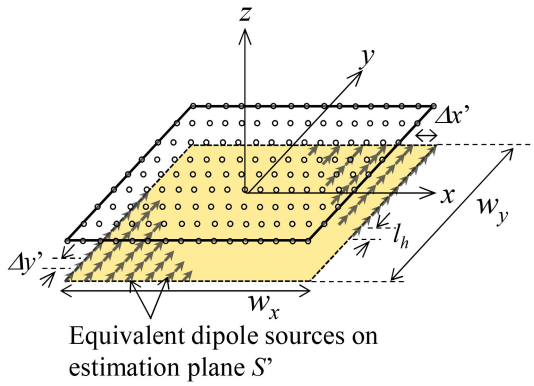

Fig. 5. Equivalent source model.

noise, whereas an ill conditioned problem is numerically unstable [16]. Therefore, the estimated equivalent current distribution from the well-conditioned problem is reliable, and vice versa. The second is the relative error between the magnitude of the y-component of the measured near-field ($= |E_y^m|$) and that of the near-field calculated from the equivalent current distribution ($= |E_y^e|$). The relative error is defined as follows:

$$\varepsilon = \frac{\sqrt{\sum_{p=1}^{P} \left(\left|E_y^m(\mathbf{r}_p)\right| - \left|E_y^e(\mathbf{r}_p)\right|\right)^2}}{\sqrt{\sum_{p=1}^{P} \left|E_y^m(\mathbf{r}_p)\right|^2}} \tag{15}$$

where $\mathbf{r}_p$ is the position vector at the pth measurement point on the measurement plane.

A. Performance of Proposed Method

The equivalent current distributions of the dipole and loop array antennas were estimated. The estimated equivalent current distributions are shown in Figs. 6 and 7. To clearly demonstrate the performance of the proposed method, the equivalent current distributions using two different approaches are also shown in these figures. The first is the conventional least-squares

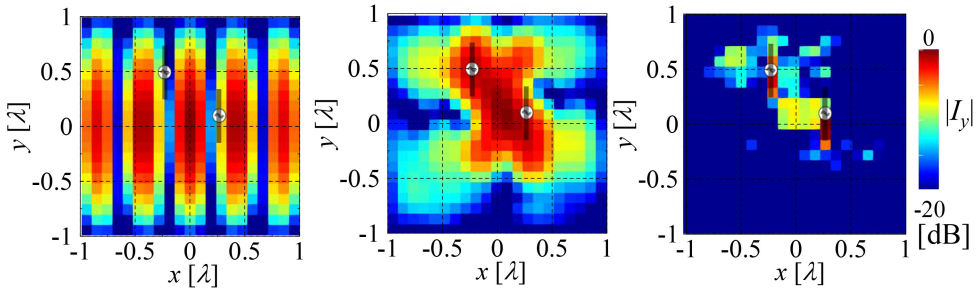

Fig. 6. Equivalent current distributions of the dipole array antenna. Left: Least-squares approach ($N = 441$, $\kappa = 7,950$, $\varepsilon = 0.79$). Center: Fourier transform ($\varepsilon = 0.43$). Right: Proposed method ($\eta = -15$ dB, $N = 146$, $L = 7$, $\varepsilon = 0.29$, $\kappa = 25.6$).

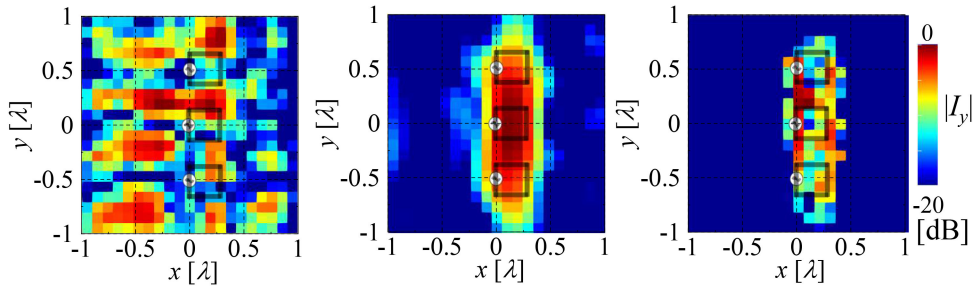

Fig. 7. Equivalent current distributions of the loop array antenna. Left: Least-squares approach ($N = 441$, $\kappa = 582.4$, $\varepsilon = 0.16$.). Center: Fourier transform ($\varepsilon = 0.26$). Right: Proposed method ($\eta = -25$ dB, $N = 96$, $L = 7$, $\varepsilon = 0.24$, $\kappa = 37$).

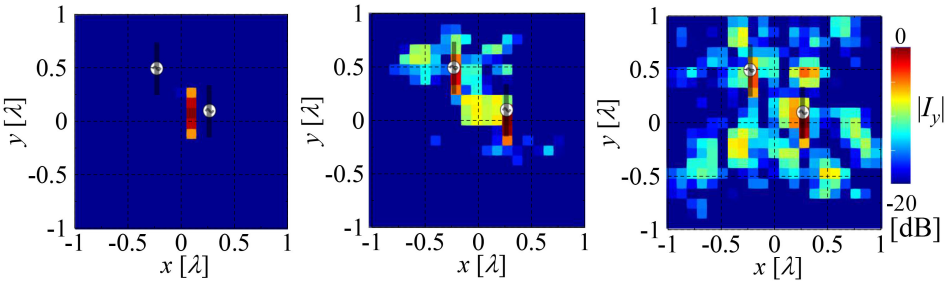

Fig. 8. Equivalent current distributions of the dipole array antenna estimated using the proposed method with different η. (Left: $\eta = -5$ dB ($N = 16L = 16\varepsilon = 0.42\kappa = 10.6$). Center: $\eta = -15$ dB ($N = 146L = 7\varepsilon = 0.29$, $\kappa = 25.6$). Right: $\eta = -20$ dB ($N = 359$, $L = 17\varepsilon = 0.24$, $\kappa = 25.4$).

approach (i.e., $\mathbf{a}_L = \{(\boldsymbol{Z}'_{P\times L})^\dagger \cdot \boldsymbol{Z}'_{P\times L}\}^{-1} \cdot (\boldsymbol{Z}'_{P\times L})^\dagger \cdot \mathbf{V}_P$), and the second is the Fourier transform based on (1)–(4). Notably, these approaches are applied to estimating the equivalent current distribution of equivalent sources without thinning (i.e., $N{=}N_i$).

As shown on the left-hand side of Figs. 6 and 7, the equivalent current distributions estimated using the conventional least-squares approach are quite different from those of real sources. Because the equivalent sources are arranged over the entire estimation plane, the total number of equivalent sources for the least-squares approach is larger than that for the proposed method. Thus, $\kappa = 7950$ for the dipole array antenna and $\kappa = 582.4$ for the loop array antenna. Therefore, it can be said that the estimation of the equivalent current distribution using the least-squares approach is ill conditioned, and the estimated equivalent current distribution is quite different from that of real sources.

The equivalent current distributions estimated using the Fourier transform are also shown at the center of Figs. 6 and 7. The amplitude of the equivalent current distribution corresponding to the position of the real source was relatively large. Therefore, the equivalent current distribution estimated using Fourier transform is coincident with the real source rather than that of the conventional least-squares approach. On the other hand, the equivalent current distribution estimated using the Fourier transform ranges over the whole entire estimation plane, and the positions of the real source cannot be clearly determined from the equivalent current distribution, especially for the dipole array antenna.

The equivalent current distributions estimated using the proposed method are also shown on the right-hand side of Figs. 6 and 7. Here, according to the parametric studies discussed later, the threshold η and number of eigenmode currents L are optimized for the two different real sources. As a result of thinning, the number of remaining equivalent sources is $N = 146$ $\left(\approx \frac{N_i}{3}\right)$ for the dipole array antenna and $N = 96$ $\left(\approx \frac{N_i}{4}\right)$ for the loop array antenna. Because the number of equivalent sources is

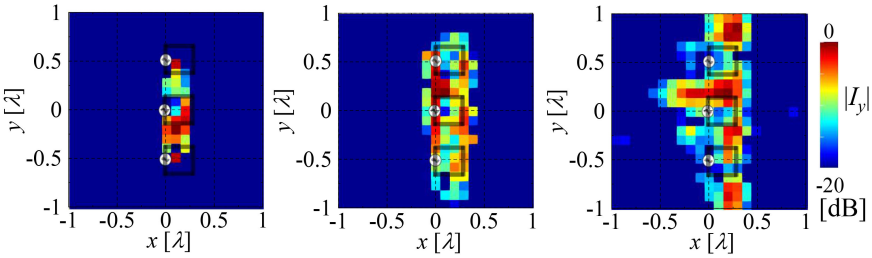

Fig. 9. Equivalent current distributions of the loop array antenna estimated using the proposed method with different η. (Left: $\eta = -15$ dB ($N = 25L = 2\varepsilon = 0.32$, $\kappa = 3.1$.) Center: $\eta = -25$ dB ($N = 96$, $L = 7$, $\varepsilon = 0.24$, $\kappa = 37$). Right: $\eta = -30$ dB ($N = 211$. $L = 9\varepsilon = 0.22$, $\kappa = 10.9$).

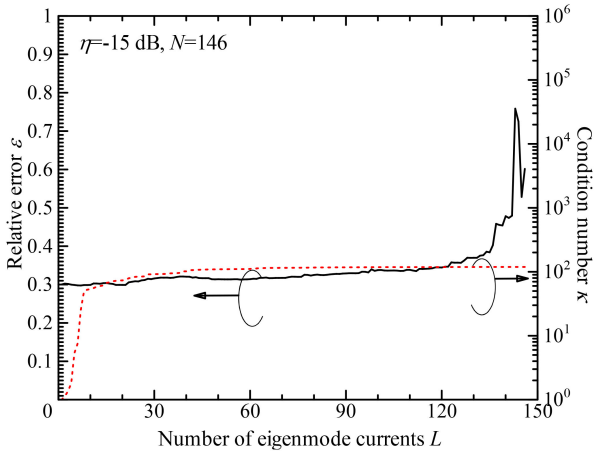

Fig. 10. Relationship among the number of eigenmode currents L, relative error ε, and condition number κ for the proposed method (dipole array antenna).

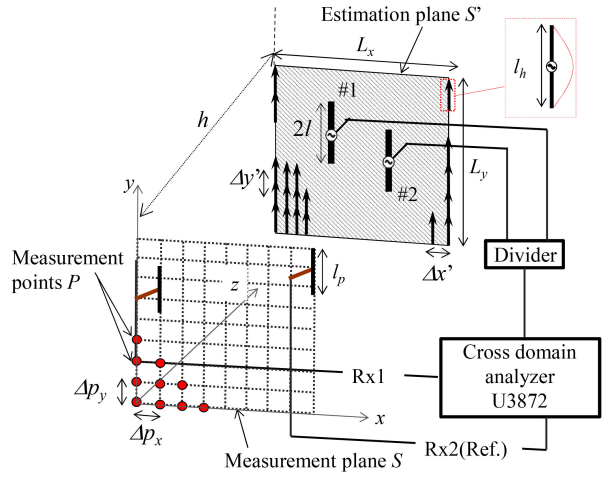

Fig. 12. Near-field measurement system for the dipole array antenna.

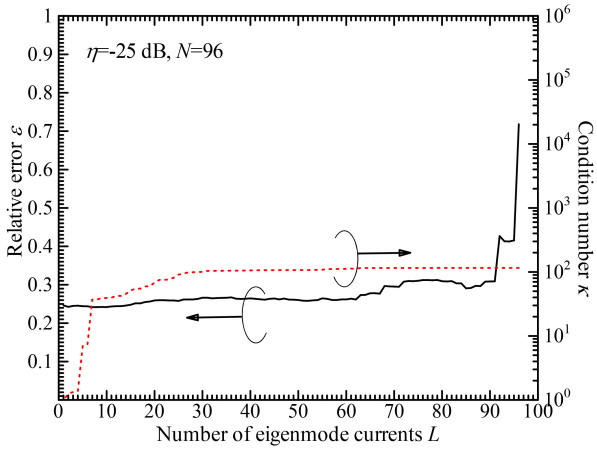

Fig. 11. Relationship among the number of eigenmode currents L, relative error ε, and condition number κ for the proposed method (loop array antenna).

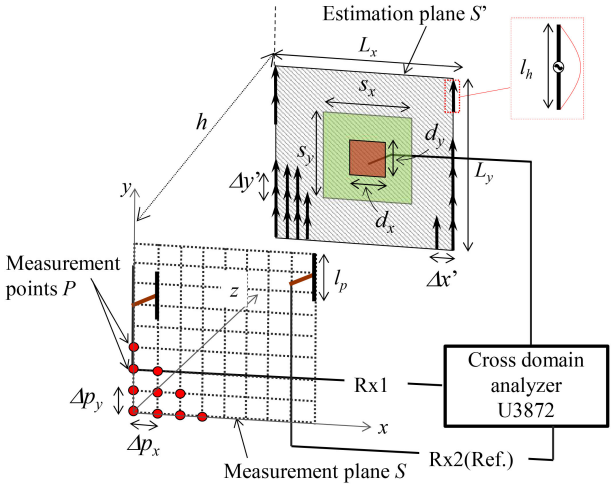

Fig. 13. Near-field measurement system for the microstrip patch antenna.

reduced, κ is reduced from 7950 to 25.6 for the dipole array antenna and from 582.4 to 37 for the loop array antenna. The equivalent current distributions estimated using the proposed method are close to real sources, whereas those estimated using the Fourier transform range over a relatively wide area of the estimation plane. Therefore, equivalent current distributions, reflecting the real sources, are successfully estimated using the proposed method.

In contrast, the near-fields from the equivalent current distributions estimated using the three different approaches were quantitatively evaluated as follows. The relative errors of the near-fields from the equivalent current distributions estimated

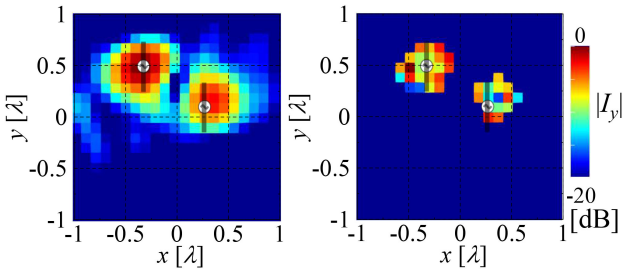

Fig. 14. Equivalent current distributions of the dipole array antenna. (Left: Fourier transform ($\varepsilon = 0.7$). Right: Proposed method ($\eta = -15$ dB$N = 38$, $L = 6$, $\varepsilon = 0.32$, $\kappa = 2.9$).

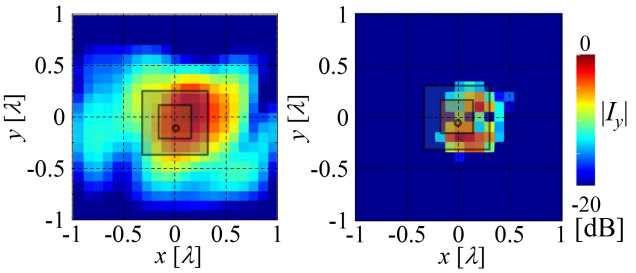

Fig. 15. Equivalent current distributions of the microstrip patch antenna. (Left: Fourier transform ($\varepsilon = 0.91$). Right: Proposed method ($\eta = -15$ dB, $N = 46$, $L = 11$, $\varepsilon = 0.45$, $\kappa = 16.6$).

using the least-squares approach, Fourier transform, and the proposed method are $\varepsilon = 0.79, 0.43$, and 0.29 for the dipole array antenna, whereas those for the loop array antenna are $\varepsilon = 0.16$, 0.26, and 0.24. Notably, the equivalent current distributions are estimated here such that their near-fields are equivalent to those of the real sources. Therefore, the relative errors of the near-fields can be small, even if the equivalent current distributions themselves are different from the real sources. For example, the equivalent current distribution of the loop array antenna estimated using the least-squares approach is quite different from the real sources, but ε of their near-fields is the smallest (=0.16). On the other hand, the equivalent current distributions estimated using the proposed method are coincident with the real sources. Moreover, ε of the near-fields from the equivalent current distribution estimated using the proposed method is the smallest (=0.29) for the dipole array antenna and is the second smallest for the loop array antenna (=0.24). Based on the discussion of the equivalent current distributions and their near-fields, it can be concluded that the proposed method enables the estimation of the equivalent current distribution reflecting the real sources without degrading the accuracy of their near-fields.

B. Parametric Studies

Here, the equivalent current distributions of the real sources were estimated using the proposed method with different thresholds, η. According to the numerical simulation, the optimum value of η is clarified from the viewpoint of mode theory. Figs. 8 and 9 show the equivalent current distributions of the real sources using the proposed method with different η values. The equivalent current distributions ranged over a relatively wide area of the estimation plane as η decreased. As mentioned earlier, the number of thinned equivalent sources becomes small when η decreases. Thus, the area where the remaining equivalent sources are arranged wides as η decreases. According to the mode theory, dominant eigenmodes of the sources correspond to their area. For example, the higher order eigenmode currents are dominant when the area of the source is larger than the wavelength and vice versa. Therefore, the optimum value of η should be given such that the area of the equivalent sources is coincident with that of the real sources. The optimum value of η was -15 dB for the dipole array antenna and -25 dB for the loop array antenna because the areas of the equivalent sources are coincident with real sources for these η values. Different optimum values of η for these real sources are attributed to their different areas. Although the precise geometry of the real sources is unknown in the proposed method, the area corresponding to the real sources can be roughly estimated from the Fourier transform.

Once the optimum value of η is determined, the remaining parameter to be determined is the number of eigenmode currents L. Figs. 10 and 11 show relationship among the number of eigenmode currents L, relative error ε, and condition number κ for the proposed method. Both ε and κ decreased as the number of eigenmode currents L decreased. The minimum ε is 0.29 for the dipole array antenna and 0.24 for the loop array antenna. The number of eigenmode currents L and condition number κ corresponding to the minimum ε are $L = 7$ and $\kappa = 25.6$ for the dipole array antenna, and $L = 7$ and $\kappa = 37$ for the loop array antenna. The parametric studies revealed that ε can be minimized when a moderate number of eigenmode currents are maintained during the estimation of the equivalent current distribution. Therefore, η and L were optimized. The equivalent current distributions shown on the right-hand side of Figs. 6 and 7 are estimated using the proposed method with the optimum parameters.

IV. Measurement Results

The performance of the proposed method was experimentally demonstrated. The first example is a two-element dipole array antenna. Similar to the numerical simulation, only the y-component of the near-field is measured, and the y-component of the equivalent current distribution is estimated. The near-field measurement system is shown in Fig. 12. The geometry of the dipole array antenna and the parameters for the measurement are described in Table I, except for the following parameters. The operating frequency of the dipole array antenna was $f = 2$ GHz. Uniform and in-phase excitations were applied to a central point of the dipole elements, namely, $(x, y) = (-0.3\lambda, 0.5\lambda)$ for element #1 and $(x, y) = (0.3\lambda, 0.1\lambda)$ for element #2. The spacing between the measurement and estimation planes was $h = 0.13\lambda$. The threshold $\eta = -15$ dB, and the resultant number of remaining equivalent sources is $N = 38$.

As a second example, the equivalent current distributions of a microstrip patch antenna were estimated, and the performance of the proposed method in a practical problem is shown. The microstrip patch antenna has been a popular antenna model in previous studies of electromagnetic compatibility [29]–[31].

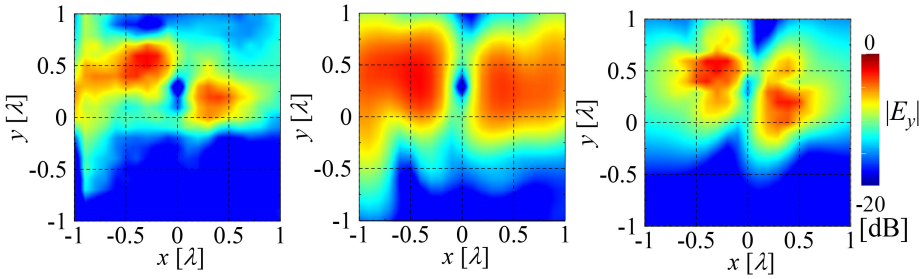

Fig. 16. Near-field distribution of the dipole array antenna. Left: Measured one of the real source. Center: Calculated one of the equivalent current distribution estimated using Fourier transform ($\varepsilon = 0.7$). Right: Calculated one of the equivalent current distribution estimated using the proposed method ($\eta = -15$ dB, $N = 38$, $L = 6$, $\varepsilon = 0.32$, $\kappa = 2.9$).

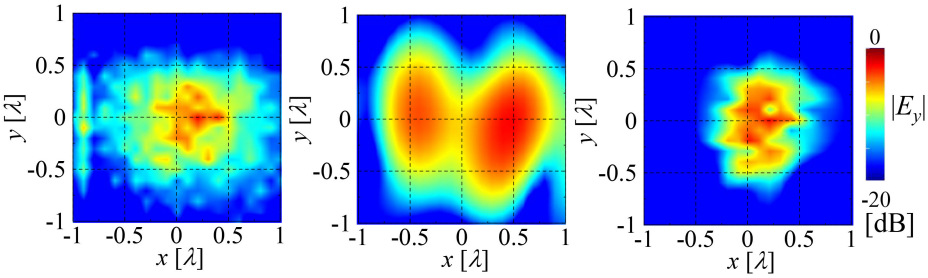

Fig. 17. Near-field distribution of the microstrip patch antenna. (Left: Measured one of the real source. Center: Calculated one of the equivalent current distribution estimated using Fourier transform ($\varepsilon = 0.91$). Right: Calculated one of the equivalent current distribution estimated using the proposed method ($\eta = -15$ dB, $N = 46$, $L = 11$, $\varepsilon = 0.45$, $\kappa = 16.6$).

A near-field measurement system for a microstrip patch antenna is shown in Fig. 13. The operating frequency of the patch antenna is $f = 2$ GHz, the size of the patch element is $d_x = d_y = 0.24\,\lambda$ and the patch element is excited by a short pin at $(x, y) = (0, -0.02\,\lambda)$. The dimensions of the substrate were $s_x = s_y = 0.5\,\lambda$. The relative permittivity of the dielectric substrate was 2.1, and the substrate was backed by a ground plane. The spacing between the measurement and estimation planes was $h = 0.2\,\lambda$. The threshold $\eta = -15$ dB, and the resultant number of remaining equivalent sources was $N = 46$. The remaining parameters, such as l_p, Δp_x, Δp_y, P, l_h, a, $\Delta x'$, $\Delta y'$, w_x, w_y, and N_i were the same as those of the near-field measurement of the dipole array antenna.

A cross-domain spectrum analyzer (Advantest U3872) was used as the two-channel RF signal receiver. The reference and measurement probes were connected to a cross-domain analyzer. The reference probe was fixed during the measurement, and its measured signal of the reference probe was used as a reference for the phase of the near-field. The dipole array antenna and microstrip patch antenna were excited using a tracking generator installed on a cross-domain analyzer. Complex near-field information is also available via an amplitude-only measurement system using a phase-retrieval technique [32].

The equivalent current distributions of the dipole array antenna estimated using the Fourier transform and proposed method are shown in Fig. 14. In addition, the equivalent current distributions of the microstrip patch antenna estimated using the Fourier transform and proposed method are shown in Fig. 15. The equivalent current distributions coincided with the real sources. However, the areas of the equivalent current distributions estimated using the Fourier transform range outside the real sources, whereas those of the proposed method are almost coincident with them. The asymmetry of the equivalent current distributions of the microstrip patch antenna may be due to the effect of fabrication errors and scattering from coaxial cables or positioners used in the measurement.

The near-field distributions of the real sources and those of the equivalent current distributions are shown in Figs. 16 and 17, respectively. For the dipole array antenna, the relative error of the near-field is $\varepsilon = 0.31$ for the proposed method, and $\varepsilon = 0.7$ for the Fourier transform. For the microstrip patch antenna, the relative error of the near-field $\varepsilon = 0.45$ for the proposed method, and 0.91 for the Fourier transform. Therefore, the near-field distributions of the equivalent current distributions obtained using the proposed method are relatively accurate compared with those obtained using the Fourier transform.

V. Conclusion

In this article, a novel estimation method for the equivalent current distribution for a source whose precise geometry is unknown is proposed. The proposed method is a hybrid method that combines the Fourier transform and eigenmode currents of equivalent sources. In the proposed method, the equivalent sources are thinned prior to determining their equivalent current distributions. Moreover, the eigenmode currents of the remaining equivalent sources are introduced, and a well-conditioned matrix equation was obtained. The equivalent current distributions of real sources were estimated numerically and experimentally using the proposed method. It has been proven that the optimum value of threshold η should be given such that the area of the equivalent sources is coincident with that of real sources.

Notably, this study demonstrated the performance of the proposed method via practical but relatively simple examples. The performance of the proposed method for complicated examples is expected to be demonstrated in the future.

APPENDIX
FOURIER TRANSFORM OF EFIE

Here, the Fourier transform of the EFIE is briefly formulated. A similar approach has been reported in the literatures [8] and [33]. To simplify the formulation, it is assumed that the y components of the current over a specific estimation plane radiate the y components of the electric field over a specific measurement plane. Both the estimation and measurement planes were assumed to be parallel to the xy plane (i.e., z and z' were constant during the formulation). According to this assumption, EFIE described in (1) can be simplified as follows:

$$E_y(x,y) = \iint_{S'} g_{yy'}(x-x,' y-y')J_y(x,' y')dS' \tag{16}$$

where

$$g_{yy'}(x-x,' y-y') = -j\omega\mu_0\left(1+\frac{1}{{k_0}^2}\frac{\partial^2}{\partial y^2}\right)\frac{e^{-jk_0|\boldsymbol{r}-\boldsymbol{r}'|}}{4\pi|\boldsymbol{r}-\boldsymbol{r}'|}. \tag{17}$$

When the Fourier transform of (16) is formulated, the Fourier transform of (1) can be formulated in the same manner.

First, the following pair of Fourier transforms and inverse Fourier transforms is introduced:

$$\tilde{f}(k_x,k_y) = \frac{1}{2\pi}\int_{-\infty}^{\infty}\int_{-\infty}^{\infty} f(x,y)e^{-jk_x x}e^{-jk_y y}dxdy \tag{18}$$

$$f(x,y) = \frac{1}{2\pi}\int_{-\infty}^{\infty}\int_{-\infty}^{\infty} \tilde{f}(k_x,k_y)e^{jk_x x}e^{jk_y y}dk_x dk_y. \tag{19}$$

When the Fourier transform shown in (18) is applied to both sides of (16), the following expression is obtained:

$$\begin{aligned}\tilde{E}_y(k_x,k_y) = &\int_{-\infty}^{\infty}\int_{-\infty}^{\infty}\int_{-\infty}^{\infty}\int_{-\infty}^{\infty} g_{yy'}(x-x',y-y')\\ &\times J_y(x',y')e^{-jk_x x}e^{-jk_y y}dxdydx'dy'.\end{aligned} \tag{20}$$

Equation (20) is a convolution integral of $g_{yy'}$ and J_y. The coordinate transformations $X = x - x'$ and $Y = y - y'$ are applied to (20) so that integrals on x' and y' coordinates are transformed into integrals on X and Y coordinates, respectively. Thus, (20) can be expressed as follows:

$$\begin{aligned}\tilde{E}_y(k_x,k_y) &= \left\{\int_{-\infty}^{\infty}\int_{-\infty}^{\infty} J_y(x',y')e^{-jk_x x'}e^{-jk_y y'}dx'dy'\right\}\\ &\quad\left\{\int_{-\infty}^{\infty}\int_{-\infty}^{\infty} g_{yy'}(X,Y)e^{-jk_x X}e^{-jk_y Y}dXdY\right\}\\ &= \tilde{J}_y(k_x,k_y)\tilde{g}_{yy'}(k_x,k_y).\end{aligned} \tag{21}$$

The Fourier transform described here was numerically performed using our in-house developed Fortran code. During the Fourier transform, the estimation plane is divided into small rectangular areas. Each rectangular area corresponded to an equivalent source. According to the formulation, the equivalent current distribution is obtained using the Fourier transform once the near-field of the real sources is measured, and the specific estimation plane is given. Therefore, the equivalent current distribution can be estimated using Fourier transform without the precise geometry of the real sources, that is, the geometry of the real sources itself does not directly affect whether the inverse problem is ill or well conditioned. Approaches based on the Fourier transform have been applied to practical inverse problems and their performance has been demonstrated [8], [34], [35].

ACKNOWLEDGMENT

The authors would like to thank staffs of Cyberscience Center, Tohoku University for their helpful advice. Discussions with the members of the Cooperative Research Project Program of the Research Institute of Electrical Communication, Tohoku University, were helpful for this work.

REFERENCES

[1] S. Shahparnia and O. M. Ramahi, "Electromagnetic interference (EMI) reduction from printed circuit boards (PCB) using electromagnetic bandgap structures," *IEEE Trans. Electromagn. Compat.*, vol. 46, no. 4, pp. 580–587, Nov. 2004.

[2] X.-Li Yang *et al.*, "A novel package lid using mushroom-type EBG structures for unintentional radiation mitigation," *IEEE Trans. Electromagn. Compat.*, vol. 60, no. 6, pp. 1882–1888, Dec. 2018.

[3] J. L. A. Quijano and G. Vecchi, "Improved-accuracy source reconstruction on arbitrary 3-D surfaces," *IEEE Antennas Wireless Propag. Lett.*, vol. 8, pp. 1046–1049, 2009.

[4] J. L. A. Quijano and G. Vecchi, "Field and source equivalence in source reconstruction on 3D surfaces," *Prog. Electromagn. Res.*, vol. 103, pp. 67–100, 2010.

[5] J. L. A. Quijano and G. Vecchi, "Near- and very near-field accuracy in 3-D source reconstruction," *IEEE Antennas Wireless Propag. Lett.*, vol. 9, pp. 634–637, 2010.

[6] P. Petre and T. K. Sarkar, "Planar near-field to far-field transformation using an equivalent magnetic current approach," *IEEE Trans. Antennas Propag.*, vol. 40, no. 11, pp. 1348–1356, Nov. 1992.

[7] A. Taaghol and T. K. Sarkar, "Near-field to near/far-field transformation for arbitrary near field geometry, utilizing an equivalent magnetic current," *IEEE Trans. Electromagn. Compat.*, vol. 38, no. 3, pp. 536–542, Aug. 1996.

[8] F. Las-Heras and T. K. Sarkar, "A direct optimization approach for source reconstruction and NF-FF transformation using amplitude-only data," *IEEE Trans. Antennas Propag.*, vol. 50, no. 4, pp. 500–510, Apr. 2002.

[9] Y. lvarez, F. Las-Heras, and M. R. Pino, "The sources reconstruction method for amplitude-only field measurements," *IEEE Trans. Antennas Propag.*, vol. 58, no. 8, pp. 2776–2781, Aug. 2010.

[10] Q. Chen, S. Kato, and K. Sawaya, "Estimation of current distribution on multilayer printed circuit board by near-field measurement," *IEEE Trans. Electromagn. Compat.*, vol. 50, no. 2, pp. 399–405, May 2008.

[11] S. Kato, Q. Chen, and K. Sawaya, "Current estimation on multi-layer printed circuit board with lumped circuits by near-field measurement," *IEICE Trans. Commun.*, vol. E91-B, no. 11, pp. 3788–3791, Nov. 2008.

[12] B. Nishina and Q. Chen, "Estimation of equivalent current distribution of modulated EM radiation source," *IEEE Trans. Antennas Propag.*, vol. 64, no. 4, pp. 1334–1341, Apr. 2016.

[13] B. Fourestie, Z. Altman, J.-C. Bolomey, J. Wiart, and F. Brouay, "Statistical model analysis applied to near-field measurements of random emissions," *IEEE Trans. Antennas Propag.*, vol. 50, no. 12, pp. 1803–1812, Dec. 2002.

[14] B. Fourestie, J.-C. Bolomey, T. Sarrebourse, Z. Altman, and J. Wiart, "Spherical near field facility for characterizing random emissions," *IEEE Trans. Antennas Propag.*, vol. 53, no. 8, pp. 2582–2589, Aug. 2005.

[15] S. Omi, T. Uno, T. Arima, and J. Wiart, "Reconstruction of internal field of dielectric objects for noninvasive SAR measurement using boundary integral equation," *IEEE Trans. Electromagn. Compat.*, vol. 61, no. 1, pp. 48–56, Feb. 2019.

[16] T. K. Sakar, D. D. Weiner, and V. K. Jain, "Some mathematical considerations in dealing with the inverse problem," *IEEE Trans. Antennas Propag.*, vol. AP-29, no. 2, pp. 373–379, Mar. 1981.
[17] T. Brown, I. Jeffrey, and P. Mojabi, "Multiplicatively regularized source reconstruction method for phaseless planar near-field antenna measurements," *IEEE Trans. Antennas Propag.*, vol. 65, no. 4, pp. 2020–2031, Apr. 2017.
[18] P. A. Barrire, J.-J. Laurin, and Y. Goussard, "Mapping of equivalent currents on high-speed digital printed circuit boards based on nearfield measurements," *IEEE Trans. Electromagn. Compat.*, vol. 51, no. 3, pp. 646–958, Aug. 2009.
[19] J. Colinas, Y. Goussard, and J. J. Laurin, "Application of the Tikhonov regularization technique to the equivalent magnetic currents nearfield technique," *IEEE Trans. Antennas Propag.*, vol. 52, no. 11, pp. 3122–3132, Nov. 2004.
[20] K. Konno, S. Asano, T. Umenai, and Q. Chen, "Diagnosis of array antennas using eigenmode currents and near-field data," *IEEE Trans. Antennas Propag.*, vol. 66, no. 11, pp. 5982–5989, Nov. 2018.
[21] K. Konno and Q. Chen, "A source reconstruction technique using eigenmode currents," in *Proc. Int. Symp. Antennas Propag.*, 2019, pp. 1–3.
[22] X. Wang, K. Konno, and Q. Chen, "Diagnosis of array antennas based on phaseless near-field data using artificial neural network," *IEEE Trans. Antennas Propag.*, vol. 69, no. 7, pp. 3840–3848, Jul. 2021.
[23] J. H. Richmond and N. Geary, "Mutual impedance of nonplanar-skew sinusoidal dipoles," *IEEE Trans. Antennas Propag.*, vol. AP-23, no. 3, pp. 412–414, May 1975.
[24] R. F. Harrington, *Field Computation by Moment Methods*. New York, NY, USA: Macmillan, 1968.
[25] D. J. Bekers, S. J. L. van Eijndhoven, A. A. F. van de Ven, P.-P. Borsboom, and A. G. Tijhuis, "Eigencurrent analysis of resonant behavior in finite antenna arrays," *IEEE Trans. Microw. Theory Tech.*, vol. 54, no. 6, pp. 2821–2829, Jun. 2006.
[26] D. J. Bekers, S. J. L. van Eijndhoven, and A. G. Tijhuis, "An eigencurrent approach for the analysis of finite antenna arrays," *IEEE Trans. Antennas Propag.*, vol. 57, no. 12, pp. 3772–3782, Dec. 2009.
[27] V. Lancellotti, B. P. de Hon, and A. G. Tijhuis, "An eigencurrent approach to the analysis of electrically large 3-D structures using linear embedding via greens operators," *IEEE Trans. Antennas Propag.*, vol. 57, no. 11, pp. 3575–3585, Nov. 2009.
[28] V. Lancellotti, B. P. de Hon, and A. G. Tijhuis, "On the convergence of the eigencurrent expansion method applied to linear embedding via greens operators (LEGO)," *IEEE Trans. Antennas Propag.*, vol. 58, no. 10, pp. 3231–3238, Nov. 2009.
[29] S.-P. Gao, H. Zhao, H.-W. Deng, B.-F. Wang, and W.-J. Zhao, "Estimating interference to airborne patch antenna with limited information," *IEEE Trans. Electromagn. Compat.*, vol. 58, no. 2, pp. 631–634, Apr. 2016.
[30] Y.-F. Shu, X.-C. Wei, R. Yang, and E.-X. Liu, "An iterative approach for EMI source reconstruction based on phaseless and single-plane near-field scanning," *IEEE Trans. Electromagnets. Compat.*, vol. 60, no. 4, pp. 937–944, Aug. 2018.
[31] Q. Huang and J. Fan, "Machine learning based source reconstruction for RF desense," *IEEE Trans. Electromagn. Compat.*, vol. 60, no. 6, pp. 1640–1647, Dec. 2018.
[32] R. G. Yaccarino and Y. R.- Samii, "Phaseless bi-polar planar near-field measurements and diagnostics of array antennas," *IEEE Trans. Antennas Propag.*, vol. 47, no. 3, pp. 574–583, Mar. 1999.
[33] J. L. Volakis and K. Sertel, *Integral Equation Methods for Electromagnetics*. Raleigh, NC, USA: SciTech Pub., 2012, pp. 66–67.
[34] P. Maheshwari, H. Kajbaf, V. V. Khilkevich, and D. Pommerenke, "Emission source microscopy technique for EMI source localization," *IEEE Trans. Electromagn. Compat.*, vol. 58, no. 3, pp. 729–737, Jun. 2016.
[35] M. Srensen, H. Kajbaf, V. V. Khilkevich, L. Zhang, and D. Pommerenke, "Analysis of the effect on image quality of different scanning point selection methods in sparse ESM," *IEEE Trans. Electromagn. Compat.*, vol. 61, no. 6, pp. 1823–1831, Dec. 2019.

Kazuto Mochiki received the B.E. and M.E. degrees in communications engineering from Tohoku University, Sendai, Japan, in 2019 and 2021, respectively.

His current research interest includes electromagnetic inverse problems.

Keisuke Konno (Member, IEEE) received the B.E. degree in communications engineering, and M.E. and D.E. degrees in electrical and communications engineering from Tohoku University, Sendai, Japan, in 2007, 2009, and 2012, respectively.

Since 2012, he has been with the Department of Communications Engineering, Graduate School of Engineering, Tohoku University, where he is currently an Associate Professor. He received a JSPS Postdoctral Fellowships for Research Abroad and he was staying with the ElectroScience Laboratory, Ohio State University, Columbus, OH, USA, as a Visiting Scholar from 2015 to 2017. His research interests include computational electromagnetics, array antennas, reflectarrays, and source reconstruction.

Dr. Konno is a member of IEICE. He was the recipient of the Encouragement Award for Young Researcher and Most Frequent Presentations Award in 2010 from the Technical Committee on Antennas and Propagation of Japan, Young Researchers Award in 2011 from the Institute of Electronics, Information and Communication Engineers (IEICE) of Japan, IEEE EMC Society Sendai Chapter Student Brush-up Session and EMC Sendai Seminar Student Best Presentation Award in 2011, JSPS Washington Director Award in 2016, MHz Rectenna Award in 2017, Young Researchers Award for ECEI of Tohoku University in 2018, Minoru Ishida Award in 2018, IEEE AP-S Japan Young Engineer Award in 2018, TOKIN Foundation Research Encouragement Award in 2019, and IEICE Communications Society Distinguished Contributions Award in 2019.

Qiang Chen (Senior Member, IEEE) received the B.E. degree in electrical engineering from Xidian University, Xi'an, China, in 1986, the M.E. and D.E. degrees in electrical engineering from Tohoku University, Sendai, Japan, in 1991 and 1994, respectively.

He is currently a Chair Professor with Electromagnetic Engineering Laboratory, Department of Communications Engineering, Faculty of Engineering, Tohoku University. His primary research interests include antennas, microwave and millimeter wave, electromagnetic measurement, and computational electromagnetics.

Dr. Chen was the recipient of the Best Paper Award and Zen-ichi Kiyasu Award in 2009 from the Institute of Electronics, Information and Communication Engineers (IEICE). He served as the Chair of IEICE Technical Committee on Photonics-Applied Electromagnetic Measurement from 2012 to 2014, the Chair of IEICE Technical Committee on Wireless Power Transfer from 2016 to 2018, the Chair of IEEE Antennas and Propagation Society Tokyo Chapter from 2017 to 2018. He is now the Chair of IEICE Technical Committee on Antennas and Propagation and a Fellow of IEICE.